

Radiance Fields from Photons

SACHA JUNGGERMAN, ARYAN GARG, and MOHIT GUPTA, University of Wisconsin-Madison, USA

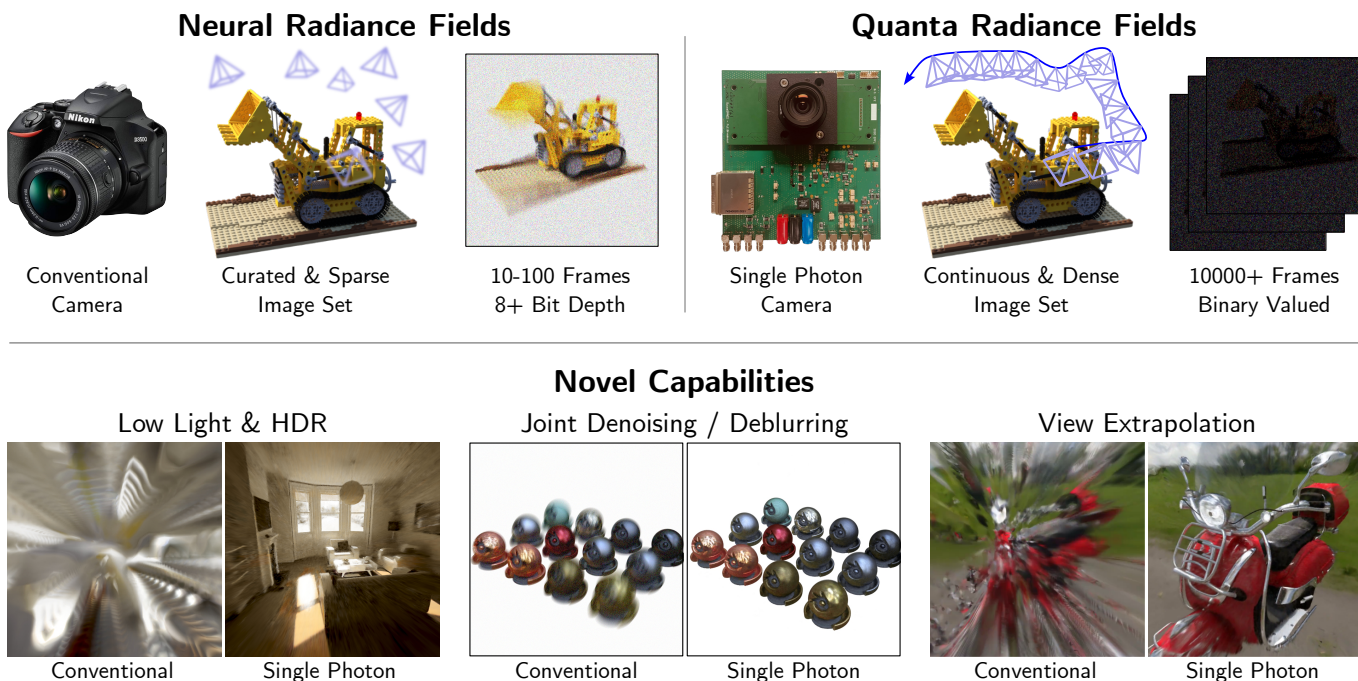


Fig. 1. **Single Photon Radiance Fields:** We introduce Quanta Radiance Fields (QRFs), neural radiance fields trained at the granularity of photons, which significantly mitigate common challenges conventional NeRFs face. They enable fast and continuous capture, enable faithful reconstructions in extremely low light and high dynamic range settings, effectively denoise and deblur training data without resorting to specialized techniques, and can produce novel view synthesis for a greater diversity of poses.

Neural radiance fields, or NeRFs, have become the de facto approach for high-quality view synthesis from a collection of images captured from multiple viewpoints. However, many issues remain when capturing images in-the-wild under challenging conditions, such as low light, high dynamic range, or rapid motion leading to smeared reconstructions with noticeable artifacts. In this work, we introduce *quanta radiance fields*, a novel class of neural radiance fields that are trained at the granularity of individual photons using single-photon cameras (SPCs). We develop theory and practical computational techniques for building radiance fields and estimating dense camera poses from unconventional, stochastic, and high-speed binary frame sequences captured by SPCs. We demonstrate, both via simulations and a SPC hardware prototype, high-fidelity reconstructions under high-speed motion, in low light, and for extreme dynamic range settings.

CCS Concepts: • **Computing methodologies** → **Volumetric models; Shape representations; Appearance and texture representations**; • **Hardware** → **Emerging optical and photonic technologies**.

Additional Key Words and Phrases: Neural Radiance Fields, Pose Estimation, Single Photon Cameras, SPADs, High-Speed Cameras, High Dynamic Range & Low-Light Imaging, Computational Imaging

Authors' Contact Information: Sacha Jungerman, sjungerman@wisc.edu; Aryan Garg, agarg54@wisc.edu; Mohit Gupta, mgupta37@wisc.edu, University of Wisconsin-Madison, Madison, WI, USA.

1 Introduction

Whether they are used for autonomous navigation, localization, or augmented and mixed reality, a cornerstone of spatially intelligent systems is the ability to represent the world around us. Neural radiance fields [55], or simply NeRFs, have recently become an attractive choice for scene representations as they capture both appearance and geometry. NeRFs fundamentally operate on a set of pixel intensity measurements that are back-projected via inverse rendering into a neural volume. From there, volumetric radiance models learn a scene representation in the form of a view-dependent pointwise color and opacity function, which produces the input pixel values when integrated along light rays.

Under favorable imaging conditions, NeRFs can be built from a set of pixel measurements (collection of images) captured using conventional cameras and can enable high-fidelity scene reconstructions. However, in real-world scenarios, pixel intensities often suffer from artifacts such as motion or optical blur, strong noise in low-light settings, saturation in high-dynamic range scenes, and non-linearities due to proprietary image sensor processing pipelines. State-of-the-art NeRF techniques suffer dramatically – or even fail entirely –

when the pixel data they consume contains such real-world imperfections. These issues are well-known and sufficiently important to have brought about long lines of work that aim to address each of these shortcomings individually [19, 20, 27, 30, 33].

We argue that many of these problems stem from the use of *pixels as the atomic measurement unit* of visual information. Since the imaging artifacts (noise, blur, saturation, non-linearities) occur when pixel values are captured, these imperfections get “baked-in” the learned radiance fields, making it extremely challenging, if not impossible, to disentangle or mitigate them after the fact.

Building Radiance Fields, One Photon at a Time: Can we take a more granular approach, and build scene representations at the granularity of individual photons – the finest scale at which visual information can be captured? If we had access to every photon in a scene, then, by definition, we would have captured the perfect radiance field, avoiding the artifacts mentioned above. Such Quanta Radiance Fields (QRF) – radiance fields built one photon at a time – would faithfully capture the photometric information in the scene, from complex specularities to varying albedoes and intricate geometry. Fortunately, there is an emerging class of single-photon cameras that are capable of detecting and counting individual photons [6, 37] at ultra-high speeds, reaching up to 100 kHz. These cameras are starting to become widely available, including in recent consumer devices (e.g., Apple iPhones), making them ideally suited to capture quanta radiance fields.

As seen in Fig. 1, by using photons as the granular unit of visual information, QRFs considerably mitigate many of the common problems that plague traditional neural radiance fields, achieving high-quality reconstructions even under extreme imaging conditions such as large motion blur or strong camera noise in low-light and high dynamic range scenes. This is most notable in extremely low flux settings where conventional NeRF reconstructions are washed out due to the sensor’s read-noise being baked into the neural volume. Furthermore, for a given total capture time, high-speed single-photon cameras sample a denser set of viewpoints, resulting in higher fidelity scene geometry estimation. This greater generalizability, referred to as view extrapolation in Fig. 1, enables novel view synthesis for views that are far from the training data. In contrast, these added viewpoints are missed by conventional cameras due to their lower frame rates leading to the characteristic cloudy or ghost-like artifacts seen in some NeRFs which are a symptom of poorly constrained geometry. Finally, with single photon cameras, one can continuously sample the scene as the camera moves through space. The resulting QRF can use the entire data sequence as input, without needing careful curation. Practically, this means that the training data can be captured considerably faster and more seamlessly, not only due to the high-speed nature of single-photon cameras but also because the user does not need to carefully plan or pause to take sharp images.

Why is it Challenging to Build QRFs? Although QRFs promise unprecedented scene representation capabilities, creating QRFs presents a unique set of challenges due to the unconventional image formation model of single-photon cameras, which capture photons as a high-speed sequence of binary frames: a pixel is “on” if at least

one photon is detected during the exposure time and “off” otherwise. Many algorithms on which neural representations rely, such as feature matching, photometric pose optimization, and volume rendering, are not directly compatible with individual binary frames which suffer from severe noise and are not directly differentiable due to their discrete (binary) nature. One could integrate long sequences of binary frames over time to lower noise and quantization, but this comes at the cost of large motion blur, thus leading to a noise-vs-blur tradeoff. Our main observation is that it is possible to simultaneously avoid both blur and noise in QRFs by dense single-photon camera pose optimization, which allows aggregating information from a large collection of binary frames. We design a novel pose optimization regularizer tailored for high-speed single-photon cameras, which enables poses corresponding to hundreds of thousands of frames to be learned simultaneously.

Another considerable challenge is that of data deluge: while QRFs are trained for the same total number of optimization steps as their traditional counterparts, their dataset is made up of 10s of thousands of noisy binary frames, as compared to a few 10s of images in traditional NeRF methods. This data volume can easily overwhelm even high-end GPUs and, even if the hardware could keep up, it can lead to training times that scale with the number of input frames which would render QRFs completely impractical. To mitigate these issues, we devise novel dataloading schemes to handle massive amounts of data captured by single-photon cameras allowing sub-linear growth of training times. In practice this scheme allows us to train QRFs with only about a 20% overhead as compared to state-of-the-art radiance field methods, making it practical to build a representation that uses individual photons as basic building blocks.

Scope and Limitations: In this work, we take the first steps towards demonstrating that building scene representations at the granularity of individual photons enables high-fidelity view synthesis and 3D reconstructions in extremely challenging scenarios that were hitherto considered impossible. Even under normal conditions, we show that quanta radiance fields enable better reconstruction and view extrapolation as compared to their conventional counterparts. Finally, we show results both using simulations and captured using our prototype single-photon camera in a wide range of imaging scenarios.

Thinking about radiance fields at the photon level may simultaneously address many of the common problems faced by neural radiance representations, however, many challenges remain. While single-photon cameras are becoming more common, this technology is not yet fully mature. Notably, current-generation sensors have limited resolution, lack color filter arrays, and incur high memory requirements. Further, although the proposed pose optimization scheme improves the reconstruction quality, poses still need to be initialized using conventional techniques. In some settings, this could become a limiting factor as conventional structure-from-motion techniques may fail before single-photon sensing. Addressing these limitations is necessary before QRFs can be widely adopted, and therefore are important next steps.

2 Related Work

Reconstruction with Single Photon Cameras: While many technologies exist that enable detecting individual photons [26], cameras based on single photon avalanche diodes (SPADs) technology are becoming prevalent due to ease of manufacturing, low cost, and high speed capture. These sensors are often used with active illumination in time-of-flight settings such as solid-state LiDARs, or for 3D reconstruction [29], however, they can also be used passively. They have been shown to have large dynamic range [14, 24], enable fast motion compensation and reconstruction [15, 28], image ultra-wideband scenes [40], and enable low-light inference [10]. In this work, we use a passive SPAD-based single-photon camera to perform 3D reconstructions and novel view synthesis.

Neural Radiance Fields: NeRFs [55] enable view synthesis by learning the scene via inverse rendering. The scene is represented implicitly and estimated by minimizing the photometric error between the observed data and a rendering of the learned scene. Many subsequent works have addressed the original shortcomings of this method, by improving its speed with spatial datastructures [32, 43], its original reliance on external pose estimates [23], or even issues regarding aliasing [1]. All these works consider a pixel as the atom of the visual representation, whereas we propose using a finer unit of visual information, the photon.

Radiance Fields for Challenging Scenes: Creating radiance fields *in-the-wild* under non-favorable imaging conditions remains challenging. Sensor noise and motion blur can result in poor reconstructions with a characteristic cloud-like appearance. Fast motion, low light, or high dynamic range can also significantly degrade reconstruction. Many methods have been developed to address these issues, although typically in a piecemeal manner. For example, a recent approach [30] trains NeRFs directly on the raw sensor data, improving low-light performance. Some methods focus on denoising by using learned priors to denoise an image sequence, treating radiance fields as a burst photography approach [33]. There are methods dedicated to deblurring, which work either by modeling motion blur as part of the inverse rendering step [20], or by using deformable kernels to correct for different types of blur [19, 27]. While these methods might be orthogonal, it is not clear if they are compatible with each other and whether they could be combined to handle multiple artifacts. Our goal is to demonstrate that, by building scene representations at the finest granularity that physics allows, QRFs can mitigate multiple challenging cases simultaneously.

3D Gaussian Splatting: Unlike NeRFs, 3D Gaussian Splatting [49] explicitly represents scenes with a collection of 3D Gaussians, bypassing the need for a deep network. These are initialized from a point cloud generated by COLMAP [34], and learnable properties like opacity and spherical harmonic coefficients [?] for color are optimized by minimizing photometric and structural errors between the observed data and the rendered scene. Subsequent works have addressed key limitations of the original method, eliminating the need for external pose estimates [7] and efficiently managing memory scaling as point density increases [9]. Others have focused on challenging conditions, such as handling motion blur [52], and improving performance in HDR and low-light scenarios [35]. While

we preliminarily explore using splatting with single photon data in section 7, this is an interesting avenue for future research.

3 Neural Radiance Fields: Background

Inverse Rendering: NeRFs learn the scene’s radiance, $L(x, d)$, and volume density, $\sigma(x)$, for any point in space, via inverse rendering, that is, they invert the process by which the scene’s radiance gets mapped to a camera pixel measurement. However, instead of integrating radiance over the solid angle subtended by each pixel and the pixel’s area, NeRFs often approximate this by taking a volumetric ray-tracing approach. The volume rendering equation used to render the expected radiant flux $\phi(r)$ incident upon a pixel parameterized by a camera ray $\mathbf{r}(t) = \mathbf{o} + t\mathbf{d}$ with near and far bounds t_n and t_f is defined as [16, 55]:

$$\phi(\mathbf{r}) = \int_{t_n}^{t_f} T(t)\sigma(\mathbf{r}(t))L(\mathbf{r}(t), \mathbf{d})dt, \quad (1)$$

where $T(t) = \exp\left(-\int_{t_n}^t \sigma(\mathbf{r}(s))ds\right)$

Directly solving for (σ, L) from a set of ideal measurements ϕ_i and their poses is intractable and is done in practice via gradient descent.

Learning Radiance Fields from Pixels: The pixel brightness I of a conventional CMOS camera can be modeled as a function of scene radiance, consisting of two simple transformations [11]. First, light passes through the camera’s optical stack, which may present aberrations and various defects. While incorrect focusing or issues with shallow depth-of-field can occur and have been the topic of recent works [19, 27], we assume this transformation is linear, or equivalently that we use an in-focus camera with aberration-free optics. The image irradiance then hits the sensor and gets converted to image brightness via a complex, nonlinear function f which encapsulates the camera response curve, tonemapping, and proprietary image signal processing. In summary, we have $I = f(\phi)$.

The specific camera response function f can vary from manufacturer to manufacturer, yet most CMOS pixels will eventually saturate as they reach their full well capacity (FWC), leading to limited dynamic range. On top of this, many sources of noise exist denoted by \mathcal{N} , which affect the sensor’s low light performance. A simple model for this response function can be written as¹:

$$I = f(\phi) = f\left(\max\left(\int_{\tau} \phi dt, \text{FWC}\right) + \mathcal{N}\right). \quad (2)$$

During training, the rendering equation Eq. 1 is computed numerically by sampling points along a ray and (σ, L) are learned by minimizing a photometric loss between the rendered pixel color $\hat{\phi}$ and the observed pixel colors I :

$$\mathcal{L}_{\text{photo}} = \|\hat{\phi} - I\|_2^2 \quad (3)$$

In so doing, we recover radiance that has the nonlinear effects of the camera response function, pixel saturation, tonemapping, and noise, baked in, as they are captured by the pixel intensities. While

¹For simplicity, various sources of noise, including photon noise, sensor read noise, fixed pattern and quantization noise, are absorbed into \mathcal{N} .

using raw linear intensity pixels can help [30], many of these issues, notably saturation, blur, and noise, remain.

4 Building Radiance Fields, One Photon at a Time

Building radiance fields from conventional pixels is limiting in three fundamental ways. First, in low flux conditions, potentially severe noise N gets baked into the learned radiance field, washing out any reconstructions. This “white noise” phenomenon can be observed in the last row of Fig. 2. Second, in high flux settings, the pixels saturate, leading to poor contrast or clipped regions. Lastly, under rapid motion or long integration times τ , pixel measurements have large motion blur. Also, for a fixed total capture time, the number of measurements will be relatively low, thus limiting the diversity of viewpoints. In this section, we develop the theoretical foundations and practical methods for estimating quanta radiance fields, i.e., radiance fields built one photon at a time, and discuss how QRFs could address the limitations described above.

4.1 Quanta Radiance Fields

We start by describing the image formation model of SPAD-based single-photon cameras that we use for capturing QRFs. SPADs are digital photon counting devices, and as such they do not suffer from read noise, making them only fundamentally shot noise limited [5]. These capabilities enable high low-light sensitivity, high temporal resolution, and extremely large dynamic range.

Consider a SPAD pixel observing a scene with a radiant flux of ϕ . The number of incident photons k on a pixel during an exposure time τ follows a Poisson distribution given by:

$$P(k) = \frac{(\phi\tau)^k e^{-\phi\tau}}{k!}. \quad (4)$$

However, a SPAD pixel resets after each photon detection. During this “dead” time, the pixel cannot detect any more photons. Thus the measurement, B , of a SPAD pixel is binary (1 if the pixel records one or more photons during exposure time τ , 0 otherwise) and follows a Bernoulli distribution given by:

$$\begin{aligned} P(B = 0) &= P(k = 0) = e^{-\phi\tau}, \\ P(B = 1) &= P(k \geq 1) = 1 - e^{-\phi\tau}. \end{aligned} \quad (5)$$

Notice how this imaging model is different from the one described by Eq. 2. There is no read-noise or full well capacity, and τ is usually in the tenths of microseconds range as opposed to the tenths of millisecond range.

Neural radiance fields from SPAD measurements: We train neural radiance fields directly on the binary measurements B_i captured with an array of SPAD pixels by defining a photometric loss term on binary measurements:

$$\mathcal{L}_{\text{quanta}} = \|\hat{\phi} - B_i\|_2^2. \quad (6)$$

Blur-Noise Tradeoff: The key challenge with estimating the radiance field directly from the above-defined loss function is the highly quantized and noisy nature of the raw binary measurements

captured by SPADs. One idea is to add a series of consecutive binary frames to generate “virtual exposures” [15] to mitigate noise and quantization. For dynamic scenes, however, this approach runs into the fundamental noise-vs-blur tradeoff. Just like a conventional camera image, if the total exposure time $n\tau$ of a virtual exposure produced by aggregating a sequence of n binary frames is large compared to the camera or scene motion, the resulting virtual exposure image will be blurred. Unlike a conventional image, however, the parameter n can be reduced post-capture by changing the exposure time after-the-fact, trading off motion blur and noise.

Instead of settling for an operating point on this blur-vs-noise tradeoff space and preprocessing groups of binary frames, we leverage the robustness to noise that optimizers provide and aggregate measurements directly in the neural volume. This can be done by using the relative pose between neighboring binary frames to reproject individual photon detections into the learned radiance field. Even though the measurements are quantized, the continuous-valued photometric loss in Eq. 6, and continuous estimated flux values, ensure the differentiability of the resulting optimization problem. When using the binary frames directly, not only can each observation be considered blur-free due to the high-speed nature of single photon cameras, but we also benefit from the largest number of differing viewpoints, which greatly helps constrain geometry.

Estimating Radiance from Quanta Measurements: Typically, NeRFs are trained using images that have been processed on-device using a complex – and often proprietary – pipeline. Previous work [30] has shown that learning a radiance field using raw, mosaicked, linear intensity images and only post-processing the re-rendered images results in cleaner denoised images and a larger dynamic range. Single photon cameras enable us to push this idea to its limit: instead of training using linear intensity images, which can be achieved using virtual exposures, we learn a radiance field directly from binary frames.

The induced change of domain on the learned radiance field means that the network learns the spatially varying, view-dependent, probability \hat{P} that at least one photon is detected. Similarly to previous works, what is learned by the network still isn’t true radiance. However, we can trivially invert the SPAD’s camera response (Eq. 5) and get a good estimate of scene radiance:

$$\hat{\phi} = -\frac{1}{\tau} \ln(1 - \hat{P}) \quad (7)$$

Note that this is similar to the maximum likelihood estimator of ϕ for a static scene [42], except here, the photon detection probability \hat{P} is estimated by the network instead of by the average of many binary frames. Using Eq. 7, we can effectively estimate the scene’s flux and render tonemapped images. Learning the photon detection probability directly avoids having to average binary frames, which might introduce motion blur and numerical instabilities that can occur in Eq. 7, and does not require any preprocessing of the raw binary data.

4.2 Data deluge & Practical Considerations

The extremely high-speed capture enabled by single photon cameras can easily strain the available bandwidth and memory of a system as a large quantity of data gets acquired rapidly. For example, a current

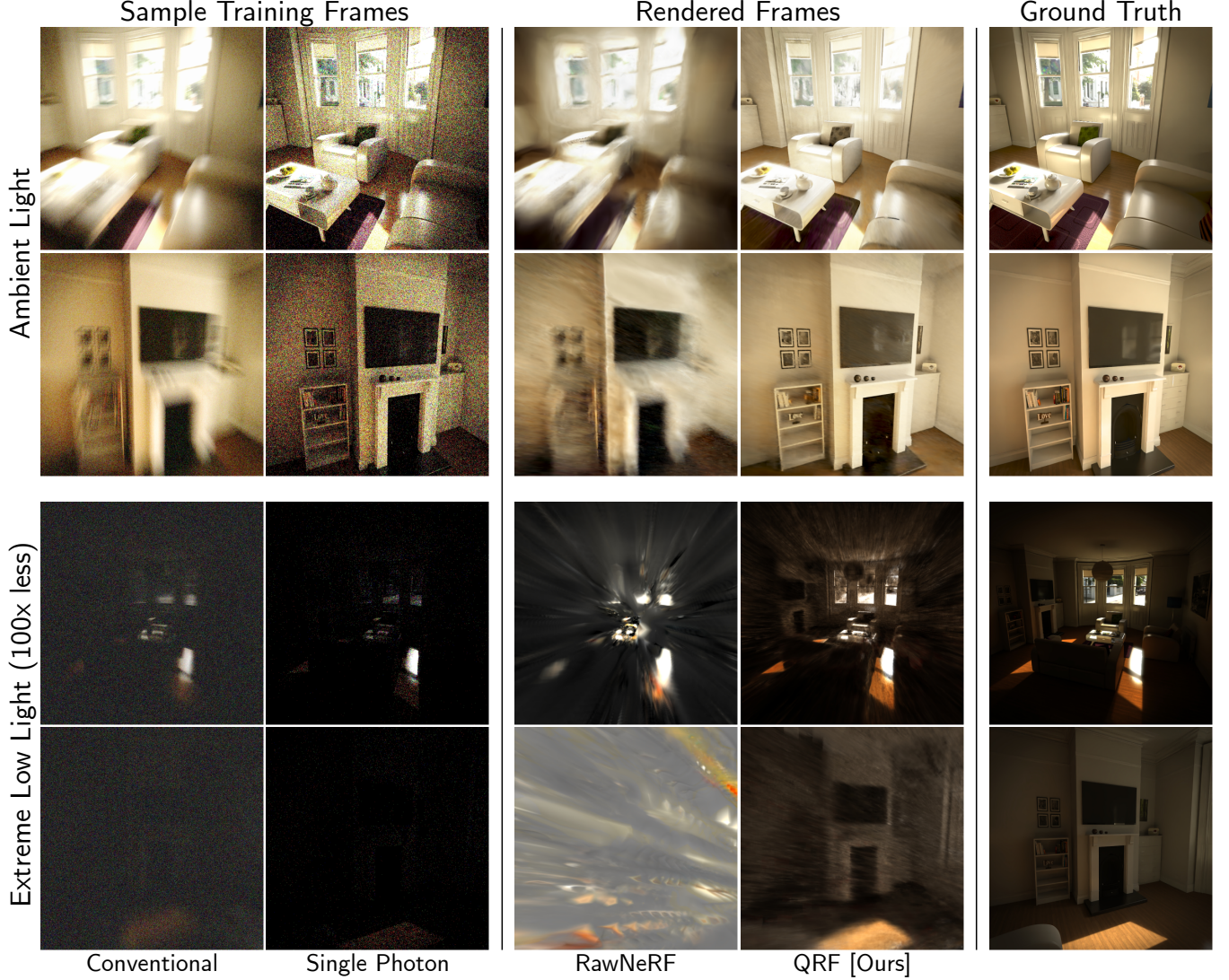


Fig. 2. **Reconstruction under challenging scenario:** We simulate a single photon and conventional camera flying through a high dynamic range scene, with a dynamic range of 16 stops, at a high speed of $\sim 72\text{km/h}$. We train a conventional NeRF with the raw, linear intensity, conventional images like in [30], and a QRF with binary frames from the simulated single-photon camera.

SPAD-based single-photon camera [37] has a modest resolution of 512×512 and can run at 100kHz, resulting in a bandwidth of 24.4 Gbps, more than two orders of magnitude (more than the 0.1 Gbps) needed for a conventional camera with similar specs running at 60 fps. This data deluge problem has been the subject of many recent works [12, 25, 36], however, these usually compress the data in a lossy way and cannot be directly used in our context for building neural scene representations.

Further, neural representations are trained on mini-batches of pairs of rays and pixel values. The implication is that at each step, a random sample of pixels must be drawn uniformly from all the training data. For conventional images this is feasible since a few hundred images can be decoded and cached on GPU as one big

tensor. However, this is infeasible for binary frames due to the prohibitively large amounts of data, thus posing an acute technical challenge.

To solve both these problems, we bit-pack the binary frames, which provides an $8\times$ compression, and memory-map the whole bit-packed array. Our dataloader is then responsible for loading binary pixel data directly from the disk, decompressing and extracting the individual bits on the fly, and sending them to the GPU. Despite training on potentially hundreds of thousands of frames, we find that, with modern solid-state drives, this data-loading scheme is only about 20% slower than when training with around a hundred conventional images that are preloaded and cached on the GPU. However, when using slower conventional hard disks the training

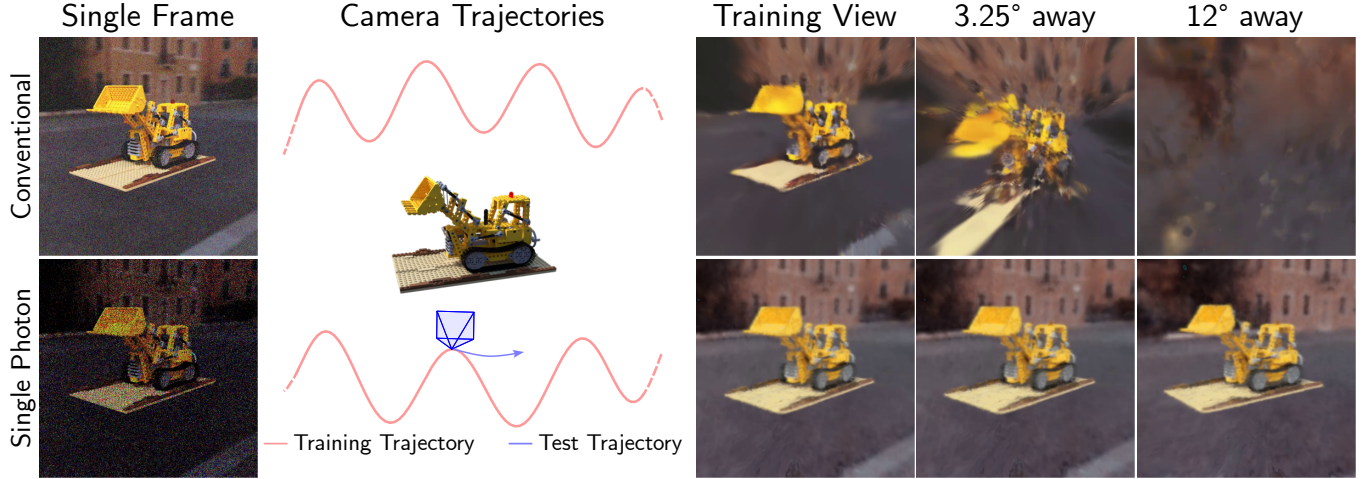


Fig. 3. **View Extrapolation:** Radiance fields trained using single photon data perform better view extrapolation and degrade more gracefully than ones trained with conventional frames, given the same total capture time. We attribute this behavior to the denser sampling of viewpoints provided by single photon cameras, which better constrains the scene’s geometry.

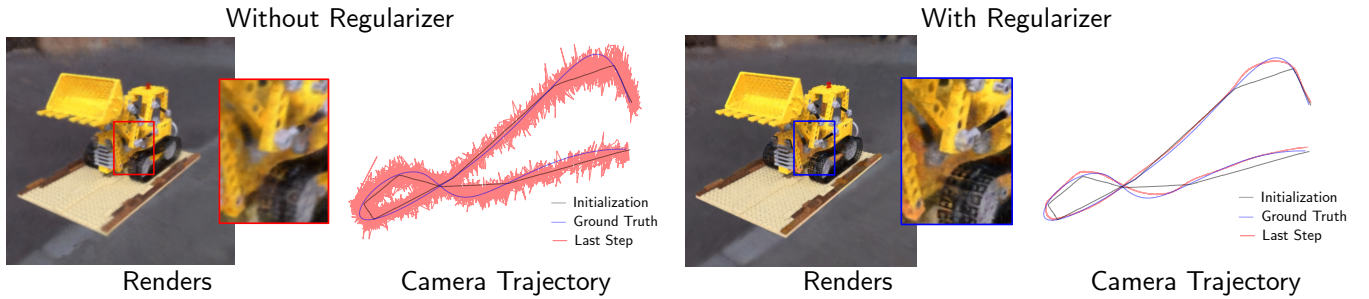


Fig. 4. **Camera Pose Optimization:** The trajectory of the camera is co-optimized with the radiance field. Due to the large number of camera poses to optimize and the noisy binary measurements, a strong smoothing regularizer on the poses is needed.

time can easily double. Bit-packing the array does not significantly impact training time, rather it makes the dataset’s disk footprint more manageable and might contribute to better cache locality.

4.3 Novel Capabilities of Quanta Radiance Fields

Low Light and High Dynamic Range: The excellent low light and high dynamic range characteristics of single-photon cameras enable the creation of neural radiance fields in challenging scenarios that are impossible to capture with conventional cameras. In Fig. 2, we simulate a conventional camera (50fps) and single photon camera (10 kHz SPAD) zipping through a scene with extremely high dynamic range ($\sim 61,000$). We show RawNeRF [30] and QRF reconstructions, as well as raw frames, for both cameras. In both cases, the trajectory and total capture time is held constant.

Under ambient light, the reconstruction trained using conventional camera frames struggles to properly reconstruct the scene due to camera motion and high dynamic range. Despite substantial noise in the single-photon input frames, the reconstruction is high-fidelity, with sharp reflections on the hardwood floor and clearly discernible books on the shelf.

Under extremely low light (100X lower than ambient light), the raw frames from both sensors are almost entirely dark, with less than 0.01 photons per pixel detected by the single photon camera. At these light levels, the read noise from the conventional camera completely overwhelms the training process, leading to distorted highlights at best, and featureless gray reconstructions at worst (last row, conventional). In contrast, the single photon reconstruction degrades much more gracefully – significant noise can be seen throughout, but the scene remains recognizable despite the extremely challenging conditions.

Denoising and Deblurring: NeRFs have been shown to be excellent general-purpose denoisers, beating even state-of-the-art one-shot denoisers, when accurate camera poses can be estimated [30]. With quanta cameras, we can take this idea to its physical limit, where the denoising and deblurring capabilities are only limited by the fundamental shot noise of photon arrival.

We demonstrate these capabilities in Fig. 2, where again, in all cases the total capture time and camera trajectories are held constant for a fair comparison. Already at medium light levels, the

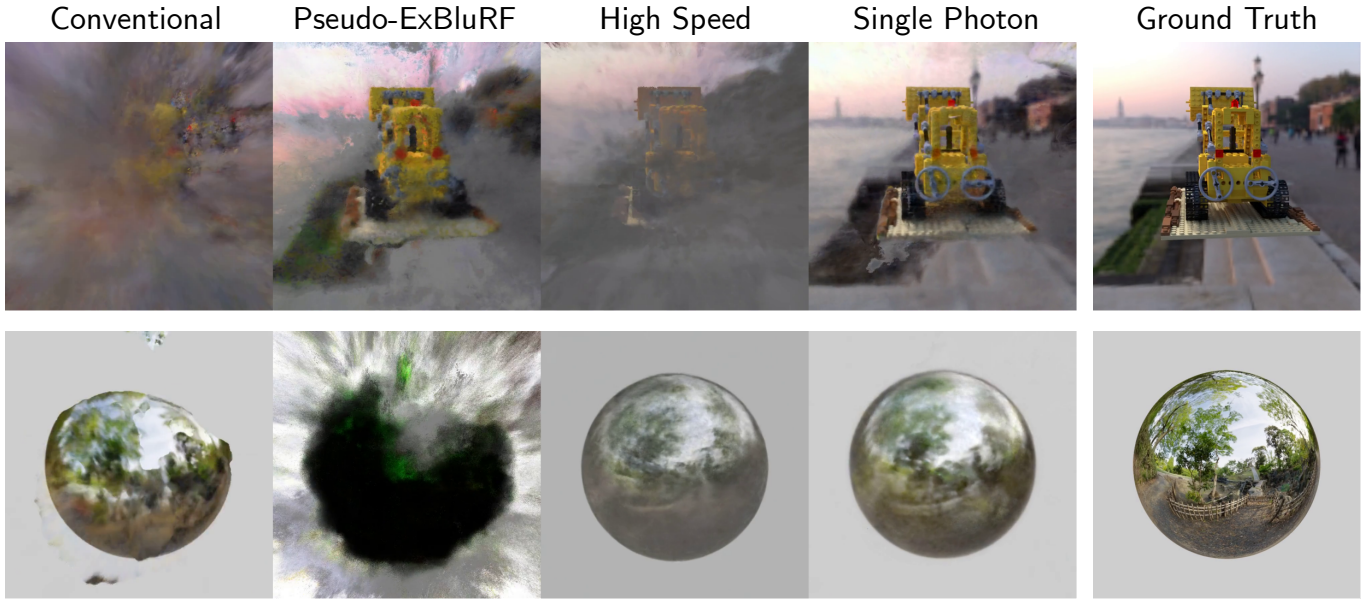


Fig. 5. **Robustness to Motion Blur:** (Column 1) Traditional NeRF reconstructions suffer considerably when the data it has been trained on contains motion blur. (Column 2) Some methods, such as [20], address this by incorporating the formation of image blur into the forward rendering model. (Column 3) A high-speed camera running at 1000fps can be used to capture more views with less motion blur, however, the colors look washed out due to the read noise being baked into the learned radiance field. (Column 4) We show that, despite much noisier individual frames, training using binary data obtained from a single photon camera achieves visually superior reconstructions.

conventional reconstructions start to suffer from motion artifacts and blown-out highlights. With 16 stops less light, reconstructions made using raw conventional camera frames are washed out due to the inherent noise in the measurements. This bias at low flux is not seen when using single photon cameras as they are only shot noise limited.

View Extrapolation: While neural radiance fields excel at novel view synthesis under ideal conditions, imperfections – such as camera noise or blur – cause typical methods to fail when the desired view is not close to a training view. We show that by using frames from a single-photon camera, which are individually noisier but can be captured at faster frame rates, enabling denser sampling and higher diversity of viewpoints, we can perform *view extrapolation* and not merely view interpolation. In Fig. 3, we learn a NeRF of a Lego truck with simulated frames for a fast conventional RGB camera (at 200fps) and a single photon camera (at 80KHz). In all cases, the total capture time and the camera’s trajectory are held constant. The training poses are drawn from a sinusoidal trajectory that encircles the object and is sampled at regular intervals corresponding to the camera’s framerate. Once trained, we render frames from a validation trajectory which starts on the training trajectory and slowly gets further along a circular arc centered on the truck. In all cases, the camera faces the truck enabling us to easily measure the displacement between the training and testing views in degrees. Here, 12° away means that the test view is exactly between two peaks in the training trajectory ($360^\circ/15$) and displaced by about one unit (radius = 5). Notice that with a small perturbation of the pose of only a few degrees, the reconstruction quality for the NeRF

trained with conventional frames degrades rapidly, and completely fails thereafter.

The training viewpoints in both cases span the same trajectory, that is, both datasets have the same pose diversity, however, the denser sampling provided by the single photon camera better constrains the scene’s geometry leading to significantly improved reconstructions.

5 Pose Optimization with Quanta Cameras

Thus far, we have assumed known camera poses, however, poses are often initialized using estimates obtained from either a structure-from-motion preprocessing step such as COLMAP [34] or from an IMU chip. As these initial estimates often suffer from noise and drift, camera poses need to be co-optimized alongside the radiance field. While most modern NeRF variants perform this optimization by default, it is not feasible when directly using binary frames. The problem is twofold: i) each individual frame is too noisy, leading to noisy optimized poses that are prone to get stuck in local minima, and ii) the number of poses that need to be optimized is greatly increased, from a few hundred to a few hundred thousand, which makes the optimization intractable.

Pose Optimization & Smoothing: Optimizing poses of conventional cameras is an already notoriously difficult and non-convex problem, which gets considerably harder when every image is binary valued as the photometric loss becomes noisy and unreliable. Our key enabling observation is that, due to the high sampling rate of single-photon cameras and known frame ordering, we can leverage a simple but powerful prior: neighboring frames should have



Fig. 6. **Additional Qualitative Evaluation on Common NeRF Datasets:** Using high-quality pretrained Zip-NeRF models [2] we emulate a single photon and conventional camera and render new training sets on which we train a baseline INGP [32] model and a QRF model respectively. While motion blur gets baked into conventional radiance fields, our method using single photon data effectively filters input noise leading to high-quality reconstructions. The type of blur that gets baked in depends on the camera trajectory, we can observe a mostly horizontal blur in the second column which is due to the orbital trajectory of the camera, while in the third column, the blur is more uniform as the camera trajectory is more complex. The last two columns have noticeably less blur since the scenes are smaller with limited camera movement.

similar poses. Specifically, the "pose trajectory" should be smooth. To formalize this insight, we devise a Fourier-domain smoothing regularizer and apply it to the pose optimization.

We first encode poses as 9-dimensional vectors consisting of a translation component $\vec{t} = [x, y, z]^T$, and a rotational component [46]. The rotational mapping is not unique, as it is overparameterized, yet it is smooth, invertible, and easily computable. The resulting tensor, \mathcal{P} , has dimensions $N \times 9$ where N is the number of poses (number of binary frames in the captured sequence).

These components are then individually smoothed using a low-pass filter in the Fourier domain, transformed back, and compared to their non-smoothed counterparts, resulting in the following total loss:

$$\hat{\mathcal{P}} = \mathcal{F}^{-1}(\mathcal{F}(\mathcal{P}) \cdot H_{\text{lowpass}})$$

$$\mathcal{L}_{\text{total}} = \mathcal{L}_{\text{quanta}} + \lambda \sum_j \|\mathcal{P}_j - \hat{\mathcal{P}}_j\|^2 \quad (8)$$

Where λ controls the regularizer strength, \mathcal{F} is the 1D Fourier transform (which is applied only along the first dimension of the pose embedding), and H_{lowpass} is the transfer function of a lowpass filter. This smoothing is performed on the 9-dimensional vectors representing camera poses. As seen in Fig. 4, a strong smoothing regularizer is imperative to get visually pleasing results when training NeRFs with high-speed binary data. With the regularizer ensuring that the overall trajectory is well-behaved, the high-speed SPAD sampling can recover fine tremors and high-frequency motion.

This frequency-based reasoning is enabled by the high sampling rate of SPADs, and is not easily applicable to conventional cameras. In fact, notice that this loss naturally degrades to the standard NeRF loss when used with conventional cameras. The total loss, $\mathcal{L}_{\text{total}}$, will

equal $\mathcal{L}_{\text{photo}}$ when the cutoff frequency of lowpass filter H_{lowpass} is larger than the Nyquist rate of the camera, which is often the case when using slow conventional RGB cameras.

Framing the regularizer in this manner allows us to think about camera shake in a natural way, using frequencies. Specifically, it enables smoothing of high-frequency motion which is mostly composed of noise. This cutoff frequency can be tuned if needed, or if any priors want to be incorporated. More complex filtering regimes are also possible, for instance, a notch filter can prove useful for filtering out specific frequencies such as vehicle resonant frequencies for vehicle-mounted cameras or handshake jitter for handheld cameras.

Deblurring as Pose Optimization: Despite potential issues caused by blurry images when optimizing for pose, for conventional cameras, motion blur and pose estimation are generally considered as two distinct issues. This is not the case for quanta radiance fields. While each individual binary frame can be assumed to have no inherent motion blur due to its extremely small exposure time, poor pose estimates will cause the learned radiance to appear blurry, while good estimates will enable a sharp reconstruction (Fig 4).

Intuitively, motion blur occurs because the inter-frame motion is not compensated. For conventional cameras, this motion cannot be easily compensated for after the fact. To circumvent this issue, modern smartphones take multiple short exposures and fuse them based on a local motion model such as optical flow [22]. We take this idea to its logical limit with extremely short exposures of single-photon imaging. With quanta radiance fields, *motion blur and pose optimization are tightly interleaved issues*, and the Fourier-regularizer introduced above helps us tackle both simultaneously.

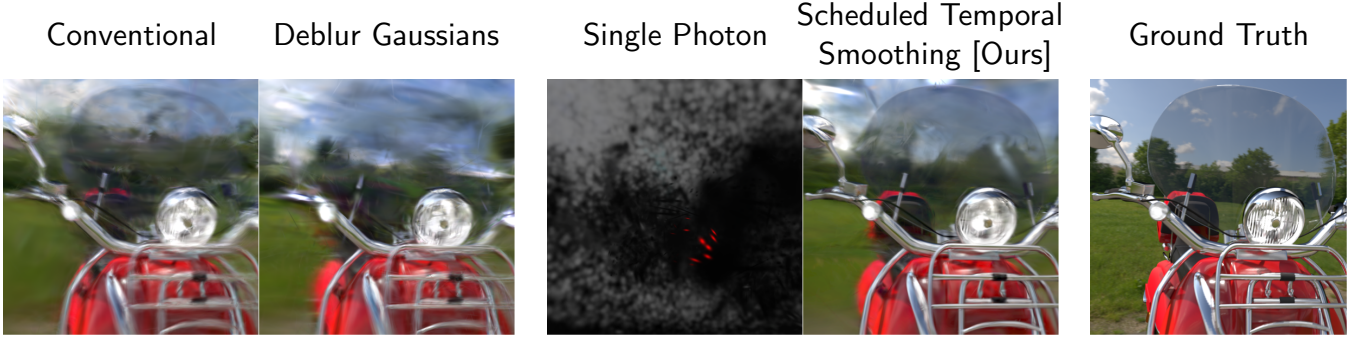


Fig. 7. **Qualitative results from explicit reconstruction:** Traditional 3D Gaussian Splatting [49] (3DGS) reconstructions suffers with motion-blur data. Deblur Gaussians [52] addresses this by modeling per-gaussian motion offsets using an MLP in the vanilla 3DGS training process. Using purely single photon data does not allow the individual gaussians to converge due to the view-dependent dynamic noise, leading to premature pruning and a failed reconstruction. However, we show that temporally smoothing single photon frames allows superior explicit 3D reconstruction.

Motion Blur Mitigation in Conventional NeRFs: Creating radiance fields out of blurry conventional images remains a challenging problem. ExBluRF [20], a state-of-the-art approach that addresses motion blur, does so by modeling blur as part of the inverse rendering process. They spawn virtual cameras into the scene and enforce that the average value seen by consecutive cameras within a certain window corresponds to the observed blurry image in the training set. Finally, they promote smooth camera movements by utilizing a Bezier curve-based regularizer term on the camera trajectory.

As this method has not yet been made publicly available, we reimplement its key features with minor modifications to perform comparisons. Specifically, we replaced their Bezier regularizer with our Fourier smoothing regularizer (Eq. 8) as they both achieve the same effect with the exception that the proposed Fourier smoothing regularizer scales to hundreds of thousands of virtual cameras. This enables a direct comparison between our method and this modified baseline, which we call pseudo-ExBluRF.

In Fig. 5, we train the pseudo-ExBluRF method with simulated 50fps images from a conventional camera and spawn 20 additional virtual cameras per training frame (corresponding to a blur kernel of 21). Camera poses are initialized to their corresponding ground truth pose, or an interpolation of them for the virtual cameras. We train our method on the equivalent dataset which would be captured by a single photon-camera capturing 40k binary frames per second, and initialize camera poses in the same way, that is, only the cameras corresponding to a 50 fps conventional camera get initialized with their true poses; every other one is initialized with an interpolated pose. Both methods use the same hyperparameters, and all camera poses are co-optimized with the radiance field. Finally, due to the slow sampling rate of the 50fps camera, the low-pass cutoff used in our regularizer is lowered to 25Hz. While one might expect a lowpass cutoff which corresponds to the Nyquist rate of the camera to not perform any filtering, this is not the case as the regularizer is applied to the virtual cameras as well which have a combined sampling rate of $50 \times 21 = 1050\text{Hz}$.

While pseudo-ExBluRF outperforms the conventional method for the Lego truck (first row of Fig. 5), it fails to recover the mirror sphere, likely due to the specularities and lack of environment

map. Better still are the reconstructions with a simulated high-speed camera, which can capture specularities, yet are washed-out due to read noise. The proposed QRFs outperform these baselines and recover accurate geometry and photometric effects, even in these challenging conditions with rapid motion and high-frequency specular reflectance.

Challenges of Simulating SPCs: Currently, simulating long SPC sequences is exorbitantly expensive, primarily due to the high frame rate of SPCs. To speed up data generation, potentially at the cost of interpolation artifacts, we use $8\times$ video interpolation using RIFE [13], allowing a full sequence of 50k – 200k frames to be rendered in less than a day. In practice, the interpolated frames are very close, thus minimizing interpolation errors.

When artifact-free or non-tonemapped renders are needed, we cannot use this shortcut as many interpolation methods do not work with HDR. For these reasons, the scenes shown in Fig. 2 were rendered completely in Blender, taking more than 20 GPU-days each to render. Interpolation was only used to create SPC datasets, not conventional ones, thus the results we show might be slightly worse than if we had artifact-free simulated SPC data.

Implementation Details: We use Nerfstudio’s implementation of Instant-NGP [32] as a backbone architecture. We use Blender [3] and Eq. 5 to simulate binary frames. Unless otherwise noted, we use a lowpass cutoff of 500Hz and a λ of 0.1. For more implementation details and code please see the supplement.

6 Quantitative Evaluations and Additional Experiments

Thus far, we have shown results only on simulated data as it enables us to emulate different image formation models and have access to ground truth. However, simulation comes at a high computational cost, with the scene shown in Fig. 2 taking more than 20 GPU days to render fully.

In section 8, we use a single photon camera hardware prototype to capture sequences and provide qualitative results on real-world experiments. Here, we instead focus on a quantitative evaluation of our method based on interpolated data from well-known NeRF datasets. This enables us to provide metrics and results on standardized scenes enabling easier comparisons to other methods.

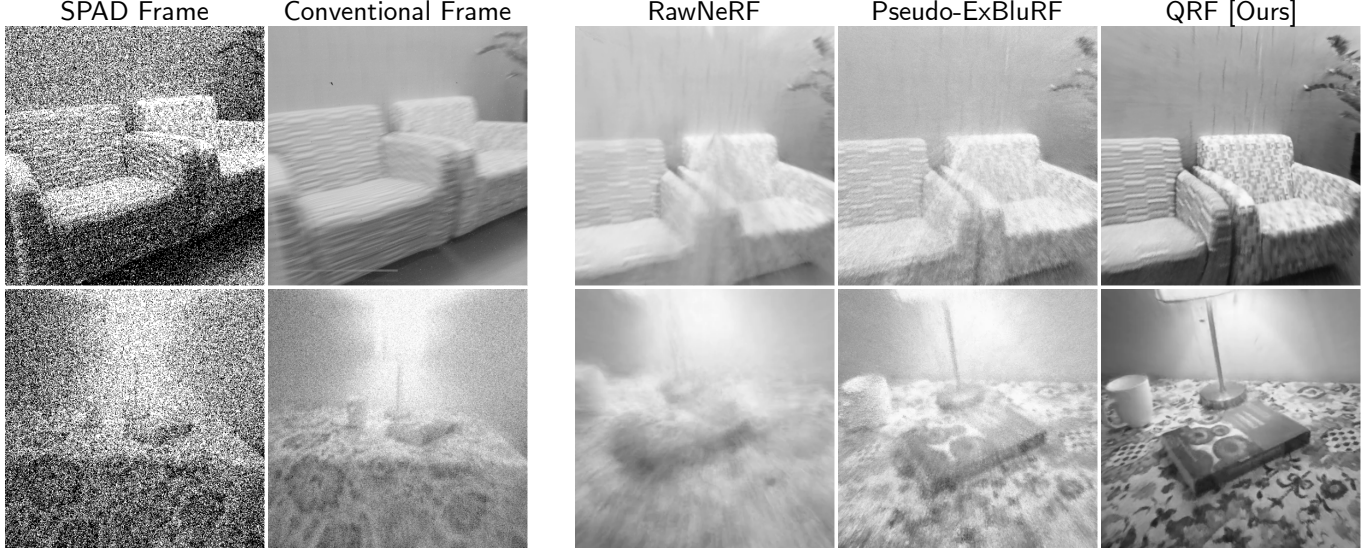


Fig. 8. **Qualitative results on real-world captures:** We capture a room-scale and tabletop scene with a single photon camera in about 8 seconds and show reconstructions made using emulated raw conventional frames at 30fps [30], a blur-specific baseline [20], and with quanta radiance fields. Overall QRFs exhibit fewer artifacts and better reconstruction quality than baseline methods.

	PSNR \uparrow	SSIM \uparrow	LPIPS \downarrow
Conventional	29.43	0.612	0.430
Single Photon	29.89	0.688	0.259
Oracle	31.62	0.880	0.075

Table 1. **Average metrics over scenes shown in Fig. 6**

Dataset Generation: Since there are no widespread datasets that have been captured with a SPC, we resort to using high quality pretrained NeRF models as a means to emulate a single photon capture. Specifically, we use pretrained Zip-NeRF models [2] (as released by SMERF [4]) and render 2000 frames along the training trajectory for each scene. From here, we either average neighboring frames in groups of 5 and apply Gaussian noise following Eq. 2 to simulate a conventional camera with realistic motion blur, or further interpolate by $16\times$ using RIFE [13] and then sample following Eq. 5 to simulate our single-photon camera. Following this procedure, we create an oracle (ground-truth) dataset consisting of 2000 static high-quality frames, a SPC dataset with 32k binary frames, and a conventional dataset with 400 RGB frames for each scene.

Evaluation Methodology: To evaluate an upper-bound performance on our new datasets, we train a standard INGP [32] model on the oracle data and report metrics computed between novel views produced by this upper-bound model and the original test set. We further train models on the conventional and single photon datasets and report metrics in Tab. 1. Despite some of these metrics being numerically close, the gap in perceptual quality is rather large as exemplified qualitatively in Fig. 6. This is especially visible in the bicycle and garden scenes where the blur captured by the conventional camera ends up being baked into the reconstruction, whereas

the QRF reconstruction is clean. We can even make the predominant direction of motion used while capturing the scenes, the bike scene was captured by moving the camera vertically, while the garden scene was captured with an circular trajectory.

7 Explicit Reconstruction

Recently, Kerbl *et al.* introduced 3D Gaussian Splatting [49], an explicitly parameterized sparse-view 3D scene reconstruction technique, that offers speed and fidelity advantages over implicit neural radiance field-based methods [1, 30, 55] when the input frames are clean. However, in less ideal conditions, for example when the capture time is limited or when the subject is poorly illuminated, it is unclear whether this explicit modeling approach achieves better or comparable performance.

In fact, many splatting works pre-process the input sequence or introduce an auxiliary network to improve the fidelity of the raw image data, rather than model the non-idealities as part of the reconstruction pipeline. For instance, HDRSplat [35] reconstructs 3D HDR scenes from low-light raw images by first denoising these raw images with a deep neural denoiser (PMRID [39]). Similarly, HO-Gaussians [53] and Deblur-Gaussians [52] introduce an MLP to process and assist the 3DGS optimization process.

When modeling the scene implicitly, the highly stochastic nature of single photon data is handled by the robustness of modern optimization techniques; the network learns the radiance that best explains the noisy observations. On the other hand, when representing the scene as an explicit collection of Gaussian blobs, what is being learned is not the radiance of a point in space but rather the position, color, and characteristics of each blob that encodes the scene. This subtle difference is responsible for splatting’s faster training and inference, but might also explain why it may not be as robust to noise as implicit methods: high view-dynamic noise patterns lead

to large gradients with respect to the Gaussian’s parameters which causes aggressive pruning or smudging of colors.

We empirically observe these adverse effects when we directly use the SPAD binary frames to represent and reconstruct the scene using splatting. As shown in Fig. 7, the reconstruction collapses and becomes largely unrecognizable. As a mitigation technique, we temporally smooth the input binary frames by averaging k neighboring frames together and decay the value of k , from multiple thousands down to 1 in a step-wise manner, during training. This scheduled temporal smoothing has the effect of reducing noise at the expense of blur early in training, leading to less premature pruning, and removing the excess blur at the cost of added noise late in training when the network is less susceptible to noise. Fig. 7 shows this method in action, and that, despite its simplicity, it achieves better results than training on conventional frames, or SPC frames alone.

8 Real World Experimental Results

We use a SwissSPAD2 [37] single-photon camera, which can be seen in Fig. 1, to validate our findings using real hardware. This SPAD-based camera is capable of reaching frame rates of 97KHz at a resolution of 512×512 . By averaging multiple consecutive binary frames, we can emulate a conventional camera running at any arbitrary slower frame rates, thus enabling direct comparisons between methods. We captured multiple scenes using this camera, two of which are shown in Fig. 8. These were taken in ~ 8 seconds at 40 kHz, the first was in ambient light while the second was only illuminated using a small nightstand lamp. From this, we emulated raw-intensity 30fps conventional frames and reconstructed the scene using multiple techniques. Again, we see higher-quality reconstruction with QRF, with other baselines having washed-out colors and noticeable artifacts.

Note that these results are in grayscale because our hardware prototype does not include a color filter array; this is a limitation of this specific device and not fundamental to SPADs. Please refer to the supplement for more details about the hardware setup and implementation details, as well as video results.

9 Discussion and Future Work

In this work, we show that learning radiance fields at the granularity of single photons has many advantages, including better view extrapolation and reconstruction quality. However, many challenges remain. Specifically, a key limitation of this approach is that, while camera poses are finetuned during training, a good initial estimate is still required. While this limitation is not unique to our method, we highlight it here as currently, this is the key limiting factor for extreme low light and in-the-wild QRFs.

Many improvements to 3D reconstruction (NeRFs and 3DGS) have been proposed, and many more will follow. New advances, from faster training and inference [8], to surface rendering approaches [38, 41], or deep priors [44, 45], could all benefit from using photons instead of pixels as their basic building blocks. These advances are orthogonal directions that will cross-pollinate with the proposed concept and systems of quanta radiance fields.

References

- [1] Jonathan T. Barron, Ben Mildenhall, Matthew Tancik, Peter Hedman, Ricardo Martin-Brualla, and Pratul P. Srinivasan. 2021. Mip-NeRF: A Multiscale Representation for Anti-Aliasing Neural Radiance Fields. *arXiv:2103.13415* [cs.CV]
- [2] Jonathan T. Barron, Ben Mildenhall, Dor Verbin, Pratul P. Srinivasan, and Peter Hedman. 2023. Zip-NeRF: Anti-Aliased Grid-Based Neural Radiance Fields. *ICCV* (2023).
- [3] Blender Online Community. 2018. Blender - a 3D modelling and rendering package. <http://www.blender.org>
- [4] Daniel Duckworth, Peter Hedman, Christian Reiser, Peter Zhizhin, Jean-François Thibert, Mario Lučić, Richard Szeliski, and Jonathan T. Barron. 2023. SMERF: Streamable Memory Efficient Radiance Fields for Real-Time Large-Scene Exploration. *arXiv:2312.07541* [cs.CV]
- [5] Neale A. W. Dutton, Istvan Gyongy, Luca Parmesan, and Robert K. Henderson. 2016. Single Photon Counting Performance and Noise Analysis of CMOS SPAD-Based Image Sensors. *Sensors* 16, 7 (2016). <https://doi.org/10.3390/s16071122>
- [6] Eric R. Fossum. 2011. The Quanta Image Sensor (QIS): Concepts and Challenges, In *Imaging and Applied Optics*. *Imaging and Applied Optics*, JTuE1. <https://doi.org/10.1364/COSI.2011.JTuE1>
- [7] Yang Fu, Sifei Liu, Amey Kulkarni, Jan Kautz, Alexei A. Efros, and Xiaolong Wang. 2024. COLMAP-Free 3D Gaussian Splatting. In *Proceedings of the IEEE/CVF Conference on Computer Vision and Pattern Recognition (CVPR)*. 20796–20805.
- [8] Stephan J Garbin, Marek Kowalski, Matthew Johnson, Jamie Shotton, and Julien Valentin. 2021. FastNeRF: High-Fidelity Neural Rendering at 200FPS. *arXiv preprint arXiv:2103.10380* (2021).
- [9] Sharath Girish, Kamal Gupta, and Abhinav Shrivastava. 2024. EAGLES: Efficient Accelerated 3D Gaussians with Lightweight EncodingS. *arXiv:2312.04564* [cs.CV] <https://arxiv.org/abs/2312.04564>
- [10] Bhavya Goyal and Mohit Gupta. 2021. Photon-Starved Scene Inference Using Single Photon Cameras. In *Proceedings of the IEEE/CVF International Conference on Computer Vision (ICCV)*. 2512–2521.
- [11] M.D. Grossberg and S.K. Nayar. 2004. Modeling the space of camera response functions. *IEEE Transactions on Pattern Analysis and Machine Intelligence* 26, 10 (2004), 1272–1282. <https://doi.org/10.1109/TPAMI.2004.88>
- [12] Felipe Gutierrez-Barragan, Atul Ingle, Trevor Seets, Mohit Gupta, and Andreas Velten. 2022. Compressive Single-Photon 3D Cameras. In *2022 IEEE/CVF Conference on Computer Vision and Pattern Recognition (CVPR)*. 17833–17843. <https://doi.org/10.1109/CVPR52688.2022.01733>
- [13] Zhewei Huang, Tianyuan Zhang, Wen Heng, Boxin Shi, and Shuchang Zhou. 2022. Real-Time Intermediate Flow Estimation for Video Frame Interpolation. In *Proceedings of the European Conference on Computer Vision (ECCV)*.
- [14] Atul Ingle, Andreas Velten, and Mohit Gupta. 2019. High Flux Passive Imaging with Single Photon Sensors. In *Proc. CVPR*.
- [15] Sacha Jungerman, Atul Ingle, and Mohit Gupta. 2023. Panoramas from Photons. In *Proceedings of the IEEE/CVF International Conference on Computer Vision (ICCV)*.
- [16] James Kajiya and Brian von Herzen. 1984. Ray Tracing Volume Densities. *ACM SIGGRAPH Computer Graphics* 18 (07 1984), 165–174. <https://doi.org/10.1145/964965.808594>
- [149] Bernhard Kerbl, Georgios Kopanas, Thomas Leimkühler, and George Drettakis. 2023. 3D Gaussian Splatting for Real-Time Radiance Field Rendering. *ACM Transactions on Graphics* 42, 4 (July 2023). <https://repo-sam.inria.fr/fungraph/3d-gaussian-splatting/>
- [52] Byeonghyeon Lee, Howoong Lee, Xiangyu Sun, Usman Ali, and Eunbyung Park. 2024. Deblurring 3D Gaussian Splatting. *arXiv:2401.00834* [cs.CV]
- [19] Dogyoon Lee, Minhyeok Lee, Chajin Shin, and Sangyoun Lee. 2023. DP-NeRF: Deblurred Neural Radiance Field With Physical Scene Priors. In *Proceedings of the IEEE/CVF Conference on Computer Vision and Pattern Recognition (CVPR)*. 12386–12396.
- [20] Dongwoo Lee, Jeongtaek Oh, Jaesung Rim, Sunghyun Cho, and Kyoung Mu Lee. 2023. ExBluRF: Efficient Radiance Fields for Extreme Motion Blurred Images. *arXiv:2309.08957* [cs.CV]
- [53] Zhuopeng Li, Yilin Zhang, Chenming Wu, Jianke Zhu, and Liangjun Zhang. 2024. HO-Gaussian: Hybrid Optimization of 3D Gaussian Splatting for Urban Scenes. *arXiv:2403.20032* [cs.CV] <https://arxiv.org/abs/2403.20032>
- [22] Orly Liba, Kiran Murthy, Yun-Ta Tsai, Tim Brooks, Tianfan Xue, Nikhil Karnad, Qiurui He, Jonathan T. Barron, Dillon Sharlet, Ryan Geiss, Samuel W. Hasinoff, Yael Pritch, and Marc Levoy. 2019. Handheld mobile photography in very low light. *ACM Transactions on Graphics* 38, 6 (Nov. 2019), 1–16. <https://doi.org/10.1145/3355089.3356508>
- [23] Chen-Hsuan Lin, Wei-Chiu Ma, Antonio Torralba, and Simon Lucey. 2021. BARF: Bundle-Adjusting Neural Radiance Fields. In *IEEE International Conference on Computer Vision (ICCV)*.
- [24] Yuhao Liu, Felipe Gutierrez-Barragan, Atul Ingle, Mohit Gupta, and Andreas Velten. 2022. Single-Photon Camera Guided Extreme Dynamic Range Imaging. In *Proceedings of the IEEE/CVF Winter Conference on Applications of Computer Vision (WACV)*. 1575–1585.

- [25] Patrick Llull, Xuejun Liao, Xin Yuan, Jianbo Yang, David Kittle, Lawrence Carin, Guillermo Sapiro, and David J. Brady. 2013. Coded aperture compressive temporal imaging. *Opt. Express* 21, 9 (May 2013), 10526–10545. <https://doi.org/10.1364/OE.21.010526>
- [26] Jiaju Ma, Saleh Masoodian, Dakota A. Starkey, and Eric R. Fossum. 2017. Photon-Number-Resolving Megapixel Image Sensor at Room Temperature without Avalanche Gain. *Optica* 4, 12 (Dec. 2017), 1474–1481. <https://doi.org/10.1364/OPTICA.4.001474>
- [27] Li Ma, Xiaoyu Li, Jing Liao, Qi Zhang, Xuan Wang, Jue Wang, and Pedro V. Sander. 2022. Deblur-NeRF: Neural Radiance Fields from Blurry Images. In *2022 IEEE/CVF Conference on Computer Vision and Pattern Recognition (CVPR)*. 12851–12860. <https://doi.org/10.1109/CVPR52688.2022.01252>
- [28] Sizhuo Ma, Shantanu Gupta, Arin C. Ulku, Claudio Brushini, Edoardo Charbon, and Mohit Gupta. 2020. Quanta Burst Photography. *ACM Transactions on Graphics (TOG)* 39, 4 (7 2020). <https://doi.org/10.1145/3386569.3392470>
- [29] Anagh Malik, Parsa Mirdehghan, Sotiris Nousias, Kiriakos N. Kutulakos, and David B. Lindell. 2023. Transient Neural Radiance Fields for Lidar View Synthesis and 3D Reconstruction. *NeurIPS* (2023).
- [30] Ben Mildenhall, Peter Hedman, Ricardo Martin-Brualla, Pratul P. Srinivasan, and Jonathan T. Barron. 2021. NeRF in the Dark: High Dynamic Range View Synthesis from Noisy Raw Images. *CoRR* abs/2111.13679 (2021). arXiv:2111.13679 <https://arxiv.org/abs/2111.13679>
- [55] Ben Mildenhall, Pratul P. Srinivasan, Matthew Tancik, Jonathan T. Barron, Ravi Ramamoorthi, and Ren Ng. 2020. NeRF: Representing Scenes as Neural Radiance Fields for View Synthesis. In *ECCV*.
- [32] Thomas Müller, Alex Evans, Christoph Schied, and Alexander Keller. 2022. Instant Neural Graphics Primitives with a Multiresolution Hash Encoding. *ACM Trans. Graph.* 41, 4, Article 102 (July 2022), 15 pages. <https://doi.org/10.1145/3528223.3530127>
- [33] Naama Pearl, Tali Treibitz, and Simon Korman. 2022. NAN: Noise-Aware NeRFs for Burst-Denoising. arXiv:2204.04668 [cs.CV]
- [34] Johannes Lutz Schönberger and Jan-Michael Frahm. 2016. Structure-from-Motion Revisited. In *Conference on Computer Vision and Pattern Recognition (CVPR)*.
- [35] Shreyas Singh, Aryan Garg, and Kaushik Mitra. 2024. HDRSplat: Gaussian Splatting for High Dynamic Range 3D Scene Reconstruction from Raw Images. *BMVC* (2024).
- [36] Varun Sundar, Andrei Ardelean, Tristan Swedish, Claudio Brushini, Edoardo Charbon, and Mohit Gupta. 2023. SoDaCam: Software-defined Cameras via Single-Photon Imaging. arXiv:2309.00066 [cs.CV]
- [37] Arin C Ulku, Claudio Brushini, Ivan Michel Antolovic, Edoardo Charbon, Yung Kuo, Rinat Ankri, Shimon Weiss, and Xavier Michalet. 2019. A 512×512 SPAD Image Sensor with Integrated Gating for Widefield FLIM. *IEEE journal of selected topics in quantum electronics : a publication of the IEEE Lasers and Electro-optics Society* 25, 1 (2019), 6801212. <https://doi.org/10.1109/jstqe.2018.2867439>
- [38] Peng Wang, Lingjie Liu, Yuan Liu, Christian Theobalt, Taku Komura, and Wenping Wang. 2023. NeuS: Learning Neural Implicit Surfaces by Volume Rendering for Multi-view Reconstruction. arXiv:2106.10689 [cs.CV]
- [39] Yuzhi Wang, Haibin Huang, Qin Xu, Jiaming Liu, Yiqun Liu, and Jue Wang. 2020. Practical Deep Raw Image Denoising on Mobile Devices. In *European Conference on Computer Vision (ECCV)*. 1–16.
- [40] Mian Wei, Sotiris Nousias, Rahul Gulve, David B Lindell, and Kiriakos N Kutulakos. 2023. Passive Ultra-Wideband Single-Photon Imaging. In *Proc. ICCV*.
- [41] Yaniv Wolf, Amit Bracha, and Ron Kimmel. 2024. GS2Mesh: Surface Reconstruction from Gaussian Splatting via Novel Stereo Views. *arXiv preprint arXiv:2404.01810* (2024).
- [42] Feng Yang, Yue M. Lu, Luciano Sbaiz, and Martin Vetterli. 2012. Bits From Photons: Oversampled Image Acquisition Using Binary Poisson Statistics. *IEEE Transactions on Image Processing* 21, 4 (2012), 1421–1436. <https://doi.org/10.1109/TIP.2011.2179306>
- [43] Alex Yu, Ruilong Li, Matthew Tancik, Hao Li, Ren Ng, and Angjoo Kanazawa. 2021. PlenOctrees for Real-time Rendering of Neural Radiance Fields. In *ICCV*.
- [44] Alex Yu, Vickie Ye, Matthew Tancik, and Angjoo Kanazawa. 2021. pixelNeRF: Neural Radiance Fields from One or Few Images. In *CVPR*.
- [45] Zhongrui Yu, Haoran Wang, Jinze Yang, Hanzhang Wang, Zeke Xie, Yunfeng Cai, Jiale Cao, Zhong Ji, and Mingming Sun. 2024. SGD: Street View Synthesis with Gaussian Splatting and Diffusion Prior. arXiv:2403.20079 [cs.CV] <https://arxiv.org/abs/2403.20079>
- [46] Yi Zhou, Connelly Barnes, Lu Jingwan, Yang Jimei, and Li Hao. 2019. On the Continuity of Rotation Representations in Neural Networks. In *The IEEE Conference on Computer Vision and Pattern Recognition (CVPR)*.

Supplementary Document for “Radiance Fields from Photons”

S.1 Simulating Single Photon Cameras

We use Blender [47] to render out ground truth RGB images of a scene for a camera moving along a spline. To save on rendering time, we only render ground truth frames at a simulated 10kHz and interpolate these to the speeds achieved by single photon cameras using [48]. This setup enables us to render a sequence in about 8 hours using a single RTX 3090.

These RGB frames are then sampled using Eq. 5 to create binary frames, or Eq. 2 to create conventional RGB frames with realistic camera a blur and noise.

S.2 Experimental Setup

Our experimental setup consists of a SwissSPAD2 [58] single-photon camera along with two Opal Kelly FPGAs, one for each half of the sensor array, and a C-Mount varifocal lens. This sensor is capable of capturing 97 thousand frames per second at a resolution of 512×512.

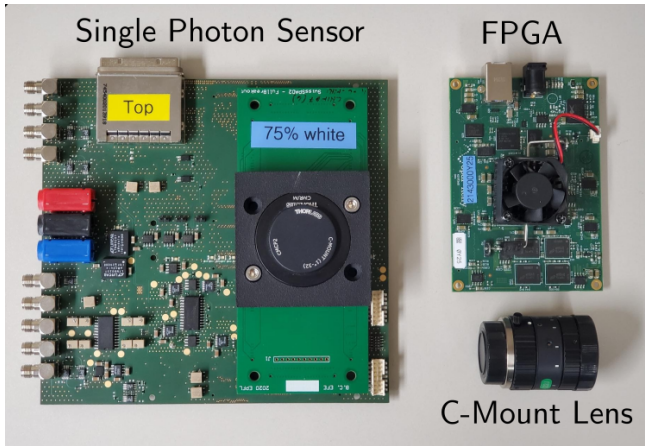


Fig. 1. Hardware Setup

In practice, we often run this sensor at slightly slower frame rates as it greatly improves the readout reliability. Using it at its maximum framerate limits the total capture time to about two seconds as the memory buffers fill up faster than the two USB 3.0 interfaces can read off.

Further, we preprocess the raw data read off this sensor by applying simple filters. First, the two half arrays are read out separately (one FPGA and USB per side), so we must recombine them after the capture is complete. Second, many pixels are dead or always on, so we apply dead-pixel and hot-pixel corrections by simply inpainting these pixels based on their neighbor’s values.

S.3 Explicit Reconstruction: 3D Gaussian Splatting

3D Gaussian Splatting (3DGS [49]) is an explicit 3D reconstruction or differentiable rasterization algorithm that achieves real-time inference speeds at desirable resolutions of 1080p. This comes at the cost of much higher representational power offered by deep network based volumetric radiance optimization algorithms like NeRFs [55] due to the explicit parameterization and no deep networks in the training procedure. We describe the 3DGS algorithm subsequently.

S.3.1 Background

Given a set of sparse views (y) alongside their camera parameters, 3D Gaussian Splatting allows optimizing the point cloud of the scene. Each point in the scene is a 3D Gaussian (G_i) in world coordinates centered at a unique position vector μ_i and is further defined by an anisotropic 3D covariance matrix (Σ) [61]:

$$G_i(x) = e^{-\frac{1}{2}(x-\mu_i)^T \Sigma_i^{-1}(x-\mu_i)} \quad (S1)$$

[61] also demonstrates projection to 2D space given a viewing transformation and derive a projected covariance matrix which is reformulated by Kerbl *et al.* [49] to

$$\Sigma = \mathcal{R} \mathcal{S} \mathcal{S}^T \mathcal{R}^T \quad (S2)$$

using scaling (\mathcal{S}) and quaternion matrices (\mathcal{R}) to satisfy the positive semi-definiteness constraint (Gaussians can not have negative scale or size) during optimization.

Finally, spherical harmonic (SH) coefficients [α] are attached to these G_i s to capture view-dependent appearances and an additional opacity scalar (α_i) is learned. After radix sorting [54] the Gaussians and projecting them to 2D space, the color of a pixel at location p is decided as follows:

$$C(p) = \sum_{i=1}^N c_i \alpha_i G'_i(p) \prod_{j=1}^{i-1} (1 - \alpha_j G'_j(p)) \quad (S3)$$

where N is the total gaussians, c_i is the color and $G'_i(p)$ is the i^{th} 3D gaussian projected to the 2D image space.

Loss: After rendering all colors/pixels for a view, an \mathcal{L}_1 and $D - SSIM$ loss is computed between the rendered and the ground truth image as follows:

$$\mathcal{L}_{3dgs} = \lambda_{dssim} \|\hat{y} - y\|_1 + (1 - \lambda_{dssim}) DSSIM(\hat{y}, y) \quad (S4)$$

We use the default $\lambda_{dssim} = 0.2$ for all our experiments.

S.3.2 Add Points Algorithm

Initializing a higher number of Gaussians per scene or starting with a denser point cloud is believed to result in superior reconstructions based on the argument that more scene details can be encoded. Extrapolating the same argument, one can theoretically populate the scene with infinite Gaussians and model the volume precisely at any granularity. Following a similar idea, Deblur Gaussians [52] introduced the Add-Points algorithm to make the point cloud dense during optimization since a dense point cloud or random initialization is not guaranteed to be dense. The algorithm simply initializes N_{extra} Gaussians and spreads them Uniformly throughout the scene. Then it uses KNN to find neighbors (4 in our case) to interpolate the

scale, rotation and color properties for optimization. This interpolation is required to not get the points pruned in the next iteration (since they are likely to receive large gradients if all parameters are randomly initialized).

S.3.3 Implementation Details

We use 3DGS’s [49] implementation that uses PyTorch [56], improvised CUDA kernels for rasterization [51] and NVIDIA CUB fast radix sort [54] for all our experiments. Additionally, we used random point cloud initializations for all experiments since it worked better overall.

The conventional camera captures are trained with default parameters except for Gaussian densification (20k) and total number of iterations (50k). This allows for encoding the scene with a much larger number of Gaussians which is beneficial for reconstruction [49, 52, 53]. The position learning rate (LR) is initialized at $1.6e^{-4}$ and is exponentially decayed to $1.6e^{-6}$. All other LRs are kept constant. Note that Adam [50] is used to optimize.

For our temporal smoothing single photon solution, we use the same hyper-parameters as above however we train with 25 fps (highest smoothing) for 20k iterations and then decay all LRs (except position which has its own exponential decay scheduler) to 50%. Subsequently, we train for another 15k iterations with 50fps smoothing and decay all other LRs to 10% of their previous value, then 10k iterations with 100fps smoothing and 5% of previous LRs step, then another 5k iterations with 200fps and 2% LRs and finally 2.5k iterations with 1000fps smoothing (less smoothing). This progressively lesser smoothing allows for adding more details (less blurring) to the scene at the cost of adding noise. However, the initial iterations help stabilize the point cloud (position, rotation and scale at least) and the decayed LRs don’t allow the Gaussians to have large gradients, which could lead to harmful pruning.

For our binary or single photon only training schedule we have to employ the Add-Points algorithm (S.3.2) from [52] to counter the aggressive pruning observed from the initial iterations. Additionally, we lower the learning rates significantly for the same reason. We initialize the position LR to 50% of the default, scaling LR at $1e^{-3}$, opacity significantly lower at $5e^{-3}$ to counter the dynamic large view-dependent noise patterns, feature LR at $5e^{-4}$, increase the spherical harmonics degree to the maximum value (3) to have the highest representation power for colors and use the Add-Points algorithm at a sample interval of 1.5k iterations. Additionally, we do not use the D-SSIM loss for binary frame training.

We use Deblur Gaussians [52] out of the box with the provided synthetic camera motion parameters to train on the (simulated) conventional camera dataset.

S.3.4 Quantitative Evaluation

We provide average PSNR, SSIM [59] and LPIPS [60] (VGG-16 [57]) metrics for the scene shown in 7 in 2. We rendered 500 frames along the same camera trajectory as a test set for all the methods.

Note that since we render in the single photon (smoothed) space, we have to transform our output from binary average to linear and then back from linear to sRGB, which allows us to compute the metrics. Assuming each binary frame was created by a Bernoulli

	PSNR↑	SSIM↑	LPIPS↓
Conventional	15.15	0.692	0.216
Deblur Gaussians	15.14	0.592	0.281
TS (Ours)	16.93	0.663	0.237

Table 2. Average metrics over the scene shown in Fig. 7

process with $p = 1 - \exp(-factor * rgb)$, then the average of binary frames tends to p . We can therefore recover the original linear intensity values as $-\log(1 - bin)/factor$. To convert this linear intensity to sRGB we use a gamma factor of 2.4.

Supplementary References

- [47] Blender Online Community. 2018. Blender - a 3D modelling and rendering package. <http://www.blender.org>
- [48] Zhewei Huang, Tianyuan Zhang, Wen Heng, Boxin Shi, and Shuchang Zhou. 2022. Real-Time Intermediate Flow Estimation for Video Frame Interpolation. In *Proceedings of the European Conference on Computer Vision (ECCV)*.
- [49] Bernhard Kerbl, Georgios Kopanas, Thomas Leimkühler, and George Drettakis. 2023. 3D Gaussian Splatting for Real-Time Radiance Field Rendering. *ACM Transactions on Graphics* 42, 4 (July 2023). <https://repo-sam.inria.fr/fungraph/3d-gaussian-splatting/>
- [50] Diederik P. Kingma and Jimmy Ba. 2014. Adam: A Method for Stochastic Optimization. *CoRR* abs/1412.6980 (2014). <https://api.semanticscholar.org/CorpusID:6628106>
- [51] Georgios Kopanas, Julien Philip, Thomas Leimkühler, and George Drettakis. 2021. Point-Based Neural Rendering with Per-View Optimization. *Computer Graphics Forum (Proceedings of the Eurographics Symposium on Rendering)* 40, 4 (June 2021). <http://www.sop.inria.fr/reves/Basilic/2021/KPLD21>
- [52] Byeonghyeon Lee, Howoong Lee, Xiangyu Sun, Usman Ali, and Eunbyung Park. 2024. Deblurring 3D Gaussian Splatting. [arXiv:2401.00834](https://arxiv.org/abs/2401.00834) [cs.CV]
- [53] Zhuopeng Li, Yilin Zhang, Chenming Wu, Jianke Zhu, and Liangjun Zhang. 2024. HO-Gaussian: Hybrid Optimization of 3D Gaussian Splatting for Urban Scenes. [arXiv:2403.20032](https://arxiv.org/abs/2403.20032) [cs.CV] <https://arxiv.org/abs/2403.20032>
- [54] Duane Merrill and Andrew S. Grimshaw. 2010. Revisiting sorting for GPGPU stream architectures. *2010 19th International Conference on Parallel Architectures and Compilation Techniques (PACT)* (2010), 545–546. <https://api.semanticscholar.org/CorpusID:14902096>
- [55] Ben Mildenhall, Pratul P. Srinivasan, Matthew Tancik, Jonathan T. Barron, Ravi Ramamoorthi, and Ren Ng. 2020. NeRF: Representing Scenes as Neural Radiance Fields for View Synthesis. In *ECCV*.
- [56] Adam Paszke, Sam Gross, Francisco Massa, Adam Lerer, James Bradbury, Gregory Chanan, Trevor Killeen, Zeming Lin, Natalia Gimelshein, Luca Antiga, Alban Desmaison, Andreas Köpf, Edward Yang, Zach DeVito, Martin Raison, Alykhan Tejani, Sasank Chilamkurthy, Benoit Steiner, Lu Fang, Junjie Bai, and Soumith Chintala. 2019. *PyTorch: an imperative style, high-performance deep learning library*. Curran Associates Inc., Red Hook, NY, USA.
- [57] Karen Simonyan and Andrew Zisserman. 2015. Very Deep Convolutional Networks for Large-Scale Image Recognition. [arXiv:1409.1556](https://arxiv.org/abs/1409.1556) [cs.CV] <https://arxiv.org/abs/1409.1556>
- [58] Arin C Ulku, Claudio Bruschini, Ivan Michel Antolovic, Edoardo Charbon, Yung Kuo, Rinat Ankri, Shimon Weiss, and Xavier Michalet. 2019. A 512×512 SPAD Image Sensor with Integrated Gating for Widefield FLIM. *IEEE journal of selected topics in quantum electronics : a publication of the IEEE Lasers and Electro-optics Society* 25, 1 (2019), 6801212. <https://doi.org/10.1109/jstqe.2018.2867439>
- [59] Zhou Wang, A.C. Bovik, H.R. Sheikh, and E.P. Simoncelli. 2004. Image quality assessment: from error visibility to structural similarity. *IEEE Transactions on Image Processing* 13, 4 (2004), 600–612. <https://doi.org/10.1109/TIP.2003.819861>
- [60] Richard Zhang, Phillip Isola, Alexei A Efros, Eli Shechtman, and Oliver Wang. 2018. The Unreasonable Effectiveness of Deep Features as a Perceptual Metric. In *CVPR*.
- [61] M. Zwicker, H. Pfister, J. van Baar, and M. Gross. 2002. EWA splatting. *IEEE Transactions on Visualization and Computer Graphics* 8, 3 (2002), 223–238. <https://doi.org/10.1109/TVCG.2002.1021576>